THE JOURNAL OF BIOLOGICAL CHEMISTRY VOL. 289, NO. 20, pp. 14225–14238, May 16, 2014


# Ras-induced Epigenetic Inactivation of the *RRAD* (Ras-related Associated with Diabetes) Gene Promotes Glucose Uptake in a Human Ovarian Cancer Model*[S]

Received for publication, October 21, 2013, and in revised form, March 19, 2014 Published, JBC Papers in Press, March 19, 2014, DOI 10.1074/jbc.M113.527671

**Yan Wang[‡§], Guiling Li[¶], Fengbiao Mao[§‖], Xianfeng Li[**], Qi Liu[¶], Lin Chen[‖], Lu Lv[¶], Xin Wang[¶], Jinyu Wu[¶], Wei Dai[‡], Guan Wang[‡‡], Enfeng Zhao[‡‡], Kai-Fu Tang[¶1], and Zhong Sheng Sun[¶‖2]**

*From the [‡]Institute of Psychology, Chinese Academy of Sciences, Beijing 100101, China, the [§]University of the Chinese Academy of Sciences, Beijing 100080, China, the [¶]Institute of Genomic Medicine, Wenzhou Medical University, 268 West Xueyuan Road, Wenzhou, Zhejiang Province 325000, China, the [‖]Beijing Institutes of Life Science, Chinese Academy of Sciences, Beijing 100101, China, the [**]State Key Laboratory of Medical Genetics, Central South University, Changsha, Hunan Province 410078, China, and the [‡‡]Department of Obstetrics and Gynecology, General Hospital of Chinese People's Liberation Army, Beijing 100853, China*

**Background:** Increased glucose uptake is essential for carcinogenesis.
**Results:** $Ras^{V12}$-induced epigenetic inactivation of RRAD promotes glucose uptake and tumor formation.
**Conclusion:** RRAD might act as a functional tumor suppressor by inhibiting glucose uptake.
**Significance:** Down-regulation of RRAD in tumor tissues might be associated with the Warburg effect.

***RRAD* (Ras-related associated with diabetes) is a small Ras-related GTPase that is frequently inactivated by DNA methylation of the CpG island in its promoter region in cancer tissues. However, the role of the methylation-induced RRAD inactivation in tumorigenesis remains unclear. In this study, the Ras-regulated transcriptome and epigenome were profiled by comparing T29H (a $Ras^{V12}$-transformed human ovarian epithelial cell line) with T29 (an immortalized but non-transformed cell line) through reduced representation bisulfite sequencing and digital gene expression. We found that $Ras^{V12}$-mediated oncogenic transformation was accompanied by *RRAD* promoter hypermethylation and a concomitant loss of RRAD expression. In addition, we found that the *RRAD* promoter was hypermethylated, and its transcription was reduced in ovarian cancer *versus* normal ovarian tissues. Treatment with the DNA methyltransferase inhibitor 5-aza-2′-deoxycytidine resulted in demethylation in the *RRAD* promoter and restored RRAD expression in T29H cells. Additionally, treatment with farnesyltransferase inhibitor FTI277 resulted in restored RRAD expression and inhibited DNA methytransferase expression and activity in T29H cells. By employing knockdown and overexpression techniques in T29 and T29H, respectively, we found that RRAD inhibited glucose uptake and lactate production by repressing the expression of glucose transporters. Finally, RRAD overexpression in T29H cells inhibited tumor formation in nude mice, suggesting that *RRAD* is a tumor suppressor gene. Our results indicate that $Ras^{V12}$-mediated oncogenic transformation induces *RRAD* epigenetic inactivation, which in turn promotes glucose uptake and may contribute to ovarian cancer tumorigenesis.***

Ras, a small 21-kDa GTPase that regulates cell proliferation and differentiation, plays a critical role in cancer initiation and progression. Mutations in genes of the human Ras family (*H-Ras*, *K-Ras*, and *N-Ras*) have been detected in ~30% of human cancers (1, 2). As a membrane protein, Ras serves as a molecular switch that mediates signal transduction across the membrane. Dysregulation of Ras signaling ultimately leads to oncogenesis (1, 3–6). Although multiple Ras effectors have been identified, the precise role of Ras in oncogenic transformation remains unclear. Dissection of Ras and other oncogene-mediated signal transduction networks is currently incomplete, probably due to lack of an appropriate human cancer model (7). Malignant epithelial carcinomas are the most common ovarian cancers and the most lethal gynecological malignancies. Although incidence of Ras mutation was observed in a subset of ovarian carcinomas (8, 9), Ras-mediated oncogenic signal transduction pathways have only recently been characterized in ovarian cancer (10–12).

T29 cells were derived from primary human ovarian surface epithelial cells by stable transfection with SV40 T/t antigens and hTERT. The immortalized but non-oncogenic T29 cells were further transformed by introducing oncogenic $HRas^{V12}$ to generate the T29H cell line, which resembles natural ovarian cancer in several aspects (10, 12). Functional proteomics analysis of Ras-mediated transformation in these cell lines enabled the identification of proteins targeted by Ras that mediate cellular metabolism, apoptosis, and the methylation pathways (10). Taking advantage of the Ras-T29H ovarian epithelial cell model, Cheng's group also found that the *OPCML* (opioid-binding protein/cell adhesion molecule-like) gene is epigenetically regulated by Ras in

* This work was supported by Natural Science Foundation of China (NSFC)-Canadian Institutes of Health Research Collaborative Research Project Grant 81161120541, National High-tech R&D Program Grant 2012AA02A202, NSFC Grants 31171236/C060503 and 31200976, Zhejiang Provincial Natural Science Foundation of China Grant Z2110521, and the Innovation Center China of AstraZeneca.
[S] This article contains supplemental Tables S1–S4.
[1] To whom correspondence may be addressed. Tel.: 86-0577-88831271; Fax: 86-0577-88831271; E-mail: tangkaifu@hotmail.com.
[2] To whom correspondence may be addressed: Beijing Institutes of Life Science, Chinese Academy of Sciences, 1 Beichen West Road, Chaoyang District, Beijing 100101, China. Tel.: 86-010-64864959; Fax: 86-010-64864959; E-mail: zhongshengsun@yeah.net.

oncogenic transformation (11). However, the genetic and epigenetic mechanisms underlying Ras involvement in oncogenic transformation remain poorly understood.

80 years ago, Otto Warburg proposed that to overcome nutrient limitations for uncontrolled cell proliferation, tumor cells exhibit an altered metabolism characterized by elevated aerobic glycolysis. This hypothesis is supported by the observation of increased glucose uptake in tumor cells (13, 14). Although aerobic glycolysis is an inefficient way to generate ATP, the ratios of ATP/ADP and ADH/$NAD^+$ are high in proliferating cells, especially when they are provided with an abundant nutrient supply in the circulating blood (13, 15, 16). When tumor cells undergo aerobic glycolysis, glucose is converted to lactate and other intermediates for biosynthesis of fatty acids, nonessential amino acids, and nucleotides (13). Numerous studies examining cancer metabolism have revealed that the genes involved in glycolysis are up-regulated in 70% of all human cancers (14, 17); however, the precise mechanisms underlying the up-regulation of aerobic glycolysis in tumor cells remain unclear.

RRAD is a member of the Ras GTPase superfamily and was first identified by its association with insulin resistance in type II diabetes mellitus (18). Accumulating evidence suggests that the *RRAD* promoter is hypermethylated in human cancers, such as nasopharyngeal carcinoma, breast cancer, malignant mesotheliomas, prostate cancer, cervical carcinoma, and lung cancer, and its promoter hypermethylation is associated with reduced RRAD expression in tumor tissues (19–25). Overexpression of RRAD in cultured adipocytes and muscle cells shows a reduction in insulin-stimulated glucose uptake (26). Ilany *et al.* (27) generated mice that overexpress RRAD in muscle and found that on a high fat diet, the transgenic mice developed more severe glucose intolerance than wild-type mice due to increased insulin resistance, and there was a further reduction in plasma triglyceride levels in the transgenic mice, which was associated with increased levels of lipoprotein lipase. These observations led us to speculate that RRAD may be involved in cancer aerobic glycolysis by regulating glucose uptake.

DNA methylation changes are integral to all aspects of cancer genomics and have been shown to have important associations with gene expression (28). In this study, the Ras-regulated transcriptome and epigenome were profiled using the $Ras^{V12}$-induced human ovarian cancer model. We found that $Ras^{V12}$-mediated oncogenic transformation was accompanied by *RRAD* promoter hypermethylation and a concomitant loss of RRAD expression. We also investigated the role of RRAD in glucose uptake and the oncogenic potential of Ras in ovarian epithelial cells.

## EXPERIMENTAL PROCEDURES

*Cell Culture, Transfection, and Stable Cell Lines*—The human ovarian epithelial cell lines T29 and T29H were generous gifts from Dr. Jinsong Liu (10, 12). 293T and HEK293 cells were obtained from the American Tissue Culture Collection (Manassas, VA). The stable cell lines T29H-G7 and T29H-G8 were established by co-transfecting T29H cells with *pCMV6-XL5 RRAD* (OriGene, Rockville, MD) and *pTK-hyg* (10:1; Clontech) followed by selection in hygromycin-containing medium (100 $\mu$g/ml). The *pCMV-RasV12* plasmid was purchased from Clontech. Plasmid transfection was performed using Lipofectamine 2000 (Invitrogen) according to the manufacturer's instructions. RRAD overexpression in stable clones was validated by real-time RT-PCR and Western blot. Cells were maintained in high glucose Dulbecco's modified Eagle's medium (DMEM) supplemented with 10% fetal bovine serum (FBS) and 1% penicillin-streptomycin and were cultured in an incubator in a 5% $CO_2$ humidified atmosphere at 37 °C.

*Bisulfite Treatment and Promoter DNA Methylation Analysis*—Genomic DNA was extracted using the genomic DNA extraction kit (TIANGEN, Beijing, China). Genomic DNA (750 ng) is used as the starting material and was converted by sodium bisulfite using the EZ DNA Methylation Kit (Zymo Research, Irvine, CA). The *RRAD* promoter region (+5 to −315 upstream of the TSS) was amplified from the modified DNA using Nest1 and Nest2 primers. The primer sequences are as follows: Nest1, 5′-GGGGTTTTAGGGTGTGTTGT-3′ (sense) and 5′-AATTCTTCTCCAAAAAACAATTAC-3′ (antisense); Nest2, 5′-GTATTGGGTTTTGGTTTTAGAGT-3′ (sense) and 5′-ACTTTTAACTAATTAAATTTACCCC-3′ (antisense). The Nest1 PCR was performed in a total volume of 20 $\mu$l using 100 ng of bisulfite-converted DNA as a template with an initial 95 °C denaturation for 5 min, followed by 32 cycles of 1-min denaturation at 95 °C, 30-s annealing at 56 °C, and 45-s extension at 72 °C. The Nest2 PCR was performed in a total volume of 35 $\mu$l containing 4.5 $\mu$l of the 10-fold diluted Nest1 PCR product under the same PCR conditions for 36 cycles. The PCR product was gel-purified, ligated into *pGEM-T* (Promega, Madison, WI), sequenced, and analyzed with the PUMA software program.

*Human Ovarian Cancer and Normal Specimens*—42 ovarian tumors and 10 normal tissues were collected from subjects who underwent surgery in The General Hospital of the People's Liberation Army (Beijing, China). Informed consent was obtained from all subjects. The protocol was approved by the Scientific Ethics Committees of The General Hospital of the People's Liberation Army. All ovarian tumors and control tissues were confirmed by the hospital's clinical pathology department. The classification and features of the ovarian tissues were as listed in Tables 1 and 2. None of the patients received chemotherapy before surgery. Tissue samples were frozen immediately in liquid nitrogen and stored at −80 °C.

*Demethylation Treatment with 5-aza-dC*[3]—T29H cells were placed in a 10-cm plate, incubated to 50% confluence, and then treated with 5-aza-dC. Growth medium was changed every 24 h. Cells were harvested after 4 days for RNA and DNA extraction, which was carried out using the TIANGEN kit (Beijing, China). The extracted RNA and DNA were then used for RRAD expression and promoter methylation analysis, respectively. Differences were analyzed by the paired *t* test using SPSS version 17.0 software. All samples were normalized to $\beta$-actin.

[3] The abbreviations used are: 5-aza-dC, 5-aza-2′-deoxycytidine; RRBS-seq, reduced representation bisulfite sequencing; DNMT, DNA methytransferase; DGE, digital gene expression; DMR, differential methylation region.

**TABLE 1**
**Classification of clinical and pathologic features**

| Characteristic | No. of patients (42 total) | No. of controls (10 total) |
|---|---|---|
| **Age** | | |
| <50 | 9 | 4 |
| 50–60 | 22 | 5 |
| >60 | 11 | 1 |
| **Differentiation** | | |
| Well | 7 | |
| Moderately | 13 | |
| Poorly | 22 | |
| **TNM stage** | | |
| I | 4 | |
| II | 4 | |
| III | 28 | |
| IV | 6 | |
| **Type** | | |
| Serous | 31 | |
| Mucinous | 5 | |
| Endometrioid | 4 | |
| Others | 2 | |

**TABLE 2**
**Individual clinical and pathologic features**

| Patient no. | Age | Type[a] | Clinical stage | Differentiation[b] | Control no. | Age |
|---|---|---|---|---|---|---|
| 1 | 57 | s | III | W | 1 | 63 |
| 2 | 73 | s | III | M | 2 | 55 |
| 3 | 55 | s | III | M | 3 | 48 |
| 4 | 64 | s | III | M | 4 | 46 |
| 5 | 55 | s | III | M | 5 | 47 |
| 6 | 54 | s | III | M | 6 | 52 |
| 7 | 54 | s | III | M | 7 | 55 |
| 8 | 53 | s | III | M | 8 | 45 |
| 9 | 52 | s | I | P | 9 | 52 |
| 10 | 48 | s | II | P | 10 | 56 |
| 11 | 37 | s | III | P | | |
| 12 | 55 | s | III | P | | |
| 13 | 53 | s | III | P | | |
| 14 | 58 | s | III | P | | |
| 15 | 45 | s | III | P | | |
| 16 | 53 | s | III | P | | |
| 17 | 68 | s | III | P | | |
| 18 | 58 | s | III | P | | |
| 19 | 38 | s | IV | P | | |
| 20 | 56 | s | IV | P | | |
| 21 | 40 | s | IV | P | | |
| 22 | 53 | s | III | W | | |
| 23 | 67 | s | III | M | | |
| 24 | 50 | s | III | M | | |
| 25 | 50 | s | III | P | | |
| 26 | 65 | s | III | M | | |
| 27 | 52 | s | III | M | | |
| 28 | 58 | s | IV | P | | |
| 29 | 47 | s | III | W | | |
| 30 | 57 | s | III | P | | |
| 31 | 63 | s | III | P | | |
| 32 | 62 | m | III | P | | |
| 33 | 47 | m | II | W | | |
| 34 | 48 | m | I | W | | |
| 35 | 47 | m | I | W | | |
| 36 | 66 | m | III | W | | |
| 37 | 64 | e | II | M | | |
| 38 | 78 | e | III | M | | |
| 39 | 66 | e | IV | P | | |
| 40 | 51 | e | II | P | | |
| 41 | 51 | o | I | P | | |
| 42 | 51 | o | IV | P | | |

[a] s, serous; m, mucinous; e, endometrioid; o, others.
[b] W, well; M, moderately; P, poorly.

**TABLE 3**
**The siRNA target sequences and RT-PCR primer sequences**

| | |
|---|---|
| **siRNA target nucleotide sequences** | |
| *siCONT* | Sense: 5′-UAACGACGCGACGACGUAATT-3′<br>Antisense: 5′-UUACGUCGUCGCGUCGUUATT-3′ |
| *siRRAD* | Sense: 5′-GCCGCAUCGUAGCUCGUAAtt-3′<br>Antisense: 5′-UUACGAGCUACGAUGCGGCcc-3′ |
| *siHRas$^{V12}$* | Sense: 5′-GGCGCCGUCGGUGUGGGCAAGtt-3′<br>Antisense: 5′-AAAAAGGGCGCCGUCGGUGUGGG CAAGtt-3′ |
| **RT-PCR primer sequences** | |
| *RRAD* | Sense: 5′-CCTGGTGCGCTCTCGTGAGGT-3′<br>Antisense: 5′-GTGCCTGCTTGCCGTCGTG-3′ |
| *HRas$^{V12}$* | Sense: 5′-GGGCGCCGTCGGTGTG-3′<br>Antisense: 5′-TCCTGAGCCTGCCGAGATTCC-3′ |
| *HRas* | Sense: 5′-GCACGCACTGTGGAATCTC-3′<br>Antisense: 5′-CGGATCTCACGCACCAAC-3′ |
| *β-actin* | Sense: 5′-GAGCTACGAGCTGCCTGACG-3′<br>Antisense: 5′-GTAGTTTCGTGGATGCCACAG-3′ |
| *DNMT1* | Sense: 5′-CCGAGTTGGTGATGGTGTGTAC-3′<br>Antisense: 5′-AGGTTGATGTCTGCGTGGTAGC-3′ |
| *DNMT3A* | Sense: 5′-TATTGATGAGCGCACAAGAGAGC-3′<br>Antisense: 5′-GGGTGTTCCAGGGTAACATTGAG-3′ |
| *DNMT3B* | Sense: 5′-GACTTGGTGATTGGCGGAA-3′<br>Antisense: 5′-GGCCCTGTGAGCAGCAGA-3′ |

*RNA Interference*—T29 or T29H cells were seeded in 6-well plates at $2.5 \times 10^5$ cells/well 1 h before transfection with siRNA and siPORT™ NeoFX™ agent (Invitrogen) according to the manufacturer's instructions. The cells were collected 72 h later. The small interfering RNAs *siRRAD* and the negative control *siCONT* were obtained from Invitrogen. *HRas$^{V12}$* siRNAs were purchased from Ambion (Austin, TX).

*Real-time Reverse Transcription PCR (RT-PCR)*—RNA was prepared using TRIzol reagent (Invitrogen) and treated with RNase-free DNase I (Fermentas, Glen Burnie, MD) for 30 min. The DNA-free RNA was reverse-transcribed using the Moloney murine leukemia virus reverse transcription kit (Promega, Madison, WI). A sample prepared in the absence of reverse transcriptase served as a negative control. SYBR Green real-time PCR was performed on an ABI PRISM 7300 sequence detection system (Applied Biosystems). Differences between samples were analyzed by independent sample *t* test using SPSS version 17.0 software. All samples were normalized to β-actin. The primer sequences for the glucose transporter have been described previously (29). The sequences of other primers used are listed in Table 3.

*Western Blotting*—Cells were collected and lysed as described (20). Lysates (80 μg) were separated by SDS-PAGE and immunoblotted with anti-RRAD antibody (Sigma). β-Actin was used as the loading control.

*DNA Methytransferase (DNMT) Activity Assay*—The nuclear extracts were prepared using the Nuclear Extraction kit (Epigentek), and then aliquotted and stored at −80 °C until the assay was performed. DNMT activity was measured using the DNMT Activity/Inhibition Assay Ultra kit (Epigentek), as described previously (30, 31). Briefly, 5-μg nuclear extracts for each assay were used as the start material, and the procedure was according to the manufacturer's instructions.

*Glucose Uptake*—Glucose uptake was determined as the accumulation of 2-deoxy-D-[$^3$H]glucose (PerkinElmer Life Sciences). Briefly, cells were rinsed twice with PBS and incubated with insulin at 37 °C for 30 min. The cells were washed twice again with PBS and incubated with 2-deoxy-D-[$^3$H]glucose (200 μM in PBS, 1 μCi/well) at 37 °C for 15 min. Cytochalasin B was used as a negative control. The reaction was terminated with three rapid washes in ice-cold PBS. The cells were lysed with 1% SDS and prepared for scintillation counting (MicroBeta-1450, PerkinElmer Life Sciences). Differences between samples were

analyzed by independent sample Student's *t* test using SPSS version 17.0 software.

*Lactate Production*—Lactate was quantified as described previously (32). Briefly, overnight cultures were harvested and resuspended in phosphate buffer containing 1 mM EDTA and sonicated to disrupt the cells. The cell debris was removed, and serial dilutions of the suspension were assayed for lactate, using the lactate assay kit from BioVision (Milpitas, CA). Lactate production was normalized to cell number. Differences between samples were analyzed by independent sample *t* test using SPSS version 17.0 software.

*Library Preparation and Sequencing of RRBS-seq*—RRBS libraries were constructed for T29 and T29H cell lines, as described previously (33). Briefly, 500 ng of genomic DNA was digested with 20 units of MspI (New England Biolabs) in a 20-$\mu$l reaction for 20 h at 37 °C. After purification, the digested products were blunt-ended, and then dA was added, followed by methylated adapter (Illumina) ligation. To obtain DNA fractions in the 40–120 and 120–220 bp range of MspI-digested products, two ranges (160–240 and 240–340 bp) of adapter-ligated fractions were excised from 2% agarose gel. The size-selected DNA was bisulfite-treated for two rounds using the EpiTect bisulfite kit (Qiagen, Venlo, The Netherlands) following the manufacturer's standard protocol. The final libraries were generated by amplification with HiFi HotStart Uracil+ ReadyMix (Kapa Biosystems, Boston, MA), and Illumina Multiplexing PCR Primers. The quality and quantity of RRBS libraries were analyzed by an Agilent 2100 Bioanalyzer (Agilent Technologies, Santa Clara, CA) and RT-PCR, respectively. Finally, Illumina HiSeq 2000 was used to sequence the libraries according to the manufacturer's protocol.

*RRBS-seq Data Analysis*—For sequencing reads produced by HiSeq 2000, the low quality reads and adapter sequences were first removed from the raw reads. The quality of resulted clean reads was checked by FastQC (available on the World Wide Web). All bisulfite-treated short reads and human reference genome sequence were then converted to three-letter alphabet. The software SOAP2 (34) was used for the alignment of the transformed reads to the transformed reference genome sequence with two mismatches allowed in the seed (40 bp) (35). To identify the position of methylcytosines and the methylation pattern of each methylcytosine, BSMAP was used to process the alignment results to identify the methylcytosines where at least three reads were covered. The detailed annotation of methylcytosines was performed using RRBS-Analyzer software (36). The cytosine methylation pattern in CpG islands across T29 and T29H sequences was determined from the mapping reads of each sample. Based on the CpG methylation pattern, the differential methylation regions (DMRs) were then identified by RRBS-Analyzer (supplemental Table S1). Two biological replicates were carried out for each cell line, and about 3.50- and 4.40-Gb 100-bp paired-end data were generated for T29 and T29H in each replicate, respectively, of which about 80% can be uniquely mapped to the human genome (supplemental Table S2). The efficiency of bisulfite treatment was evaluated by calculating the C to T conversion rate for all cytosines in the CpH context (CpA, CpC, or CpT dinucleotides). It was shown that the bisulfite conversion rates of both libraries were at least 99.80% even if we assumed that all 5mC in CpH dinucleotides were due to conversion failure, which maintained the false positive rate below 0.5%. In addition, we observed that the Pearson correlations were about ~0.95 within intrareplicate from both cell lines, indicating the high quality of our RRBS procedures (data not shown).

*DGE Library Preparation and Sequencing*—DGE libraries from both T29 and T29H cells were prepared by using the Illumina Gene Expression Sample Prep kit. Briefly, mRNA for each sample was reverse-transcripted to cDNA. Then the resulting cDNAs were ligated to sequencing adapters, and the products were purified and enriched with PCR to create the final cDNA libraries, which were then sequenced using the Illumina GAII System.

*DGE Data Analysis*—The raw data were initially filtered by removing adapters, empty reads, and low quality tags. All clean tags were then mapped to the human reference sequences using Bowtie (37) with a maximum 1-bp mismatch allowed. The clean tags that mapped to multiple sites of reference sequences were filtered, and the remaining clean tags were designated as unambiguous clean tags. The number of unambiguous clean tags for each gene was calculated and then normalized to number of transcripts per million clean tags (38). To compare the gene expression between T29 and T29H cells statistically, the false discovery rate was used to determine the statistical significance in multiple tests. An absolute value of the $\log_2$ ratio $>1$ and a false discovery rate $<0.0001$ were used as the thresholds to determine significant differences in gene expression (39). The differentially expressed genes were chosen for the KEGG pathway and GO enrichment analyses by using the ClueGO plugin in Cytossape. A Bonferroni corrected $p$ value of $<0.05$ based on right-sided hypergeometric tests was selected as the threshold for significant pathway/GO enrichment of the gene sets.

*Tumor Growth Assay*—All animal experiments were approved by the Animal Care and Use Committee at the Institute of Psychology, Chinese Academy of Sciences (Beijing, China) and were conducted in accordance with the standard animal operating procedures by following the animal welfare guidelines. Cells ($2.5 \times 10^6$; T29H-G7, T29H-G8, T29, and T29H) were harvested and resuspended in 0.1 ml of PBS. The suspensions were then injected subcutaneously into the abdomen of 5-week-old male nude mice. Each treatment group contained five mice. Tumors were measured with calipers in three dimensions once a week. The entire experiment was halted 6 weeks later when all T29H-injected mice had a visible tumor (>15 mm) in a single dimension. Differences between groups of cells or between sets of *in vitro* experiments were analyzed by one-way analysis of variance and then by Student's *t* test.

*Statistical Analysis*—Expression differences in clinical tissue samples were analyzed by the non-parametric Mann-Whitney *U* test, using SPSS version 17.0 software. Data are displayed as means ± S.E. Statistical significance was accepted at $p < 0.05$ when compared with the corresponding control or as specifically indicated.

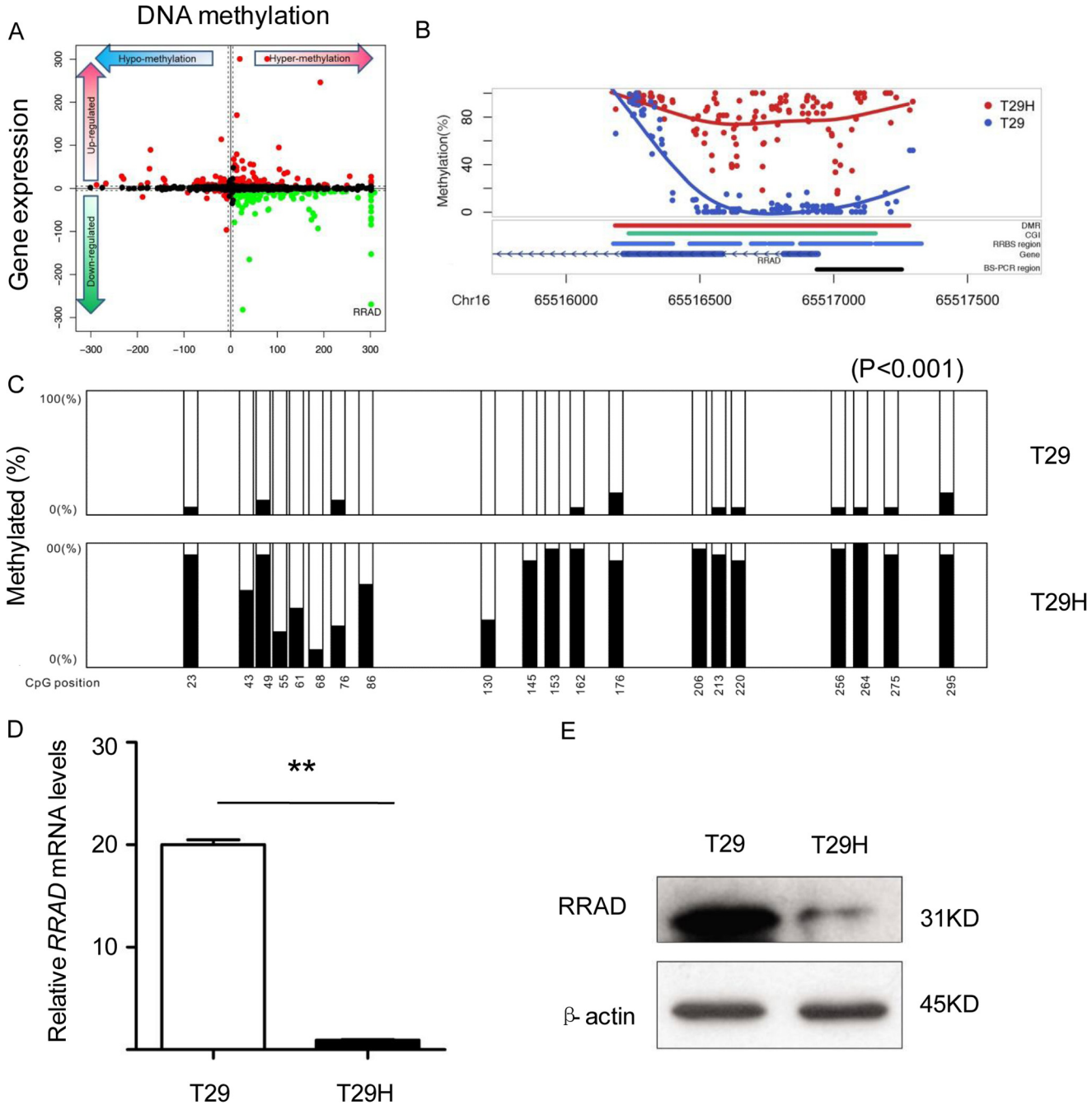


FIGURE 1. **RRAD DNA methylation is inversely correlated with expression in cultured ovarian epithelial cells.** *A*, starburst plot showing the association between DMRs in the promoter and the gene expression level. *B*, detailed view of DMR of RRAD from the RRBS-seq data. *C*, DNA methylation status of the *RRAD* promoter in T29 and T29H cells (***, $p < 0.001$). *D*, reduced *RRAD* mRNA levels in T29H *versus* T29 cells. *E*, reduced RRAD protein levels in T29H cells. Data are shown as means ± S.E. (*error bars*) (**, $p < 0.01$); β-actin was used as an internal control.

## RESULTS

*RRAD DNA Methylation Is Inversely Correlated with Expression in Cultured Ovarian Cell Models*—To profile the Ras-regulated epigenome, we performed RRBS-seq, which allows quantitative measurement of the DNA methylation levels at single-base resolution in the T29 and T29H cell lines. It was revealed that our RRBS-seq data have covered 14.17 and 14.90% of all of the 56.33 million CpG in the whole human genome for T29 and T29H, respectively. For the CpG locating in the CpG islands, 46.91 and 47.35% of them have been covered.

DNA methylation changes within the promoter region of a given gene are likely to regulate its expression level. We then measured the mRNA expression profiles of T29 and T29H using the DGE method (40). Initially, a total of 6,341,442 and 5,747,842 raw sequence reads were produced for T29 and T29H, respectively. To determine the expression level of each gene, the counts of reads aligned to the human genome were calculated and normalized by the total reads of each cell line and standardized to reads per million. In comparison with T29, 1,963 differentially expressed genes, including 1,354 up-regu-

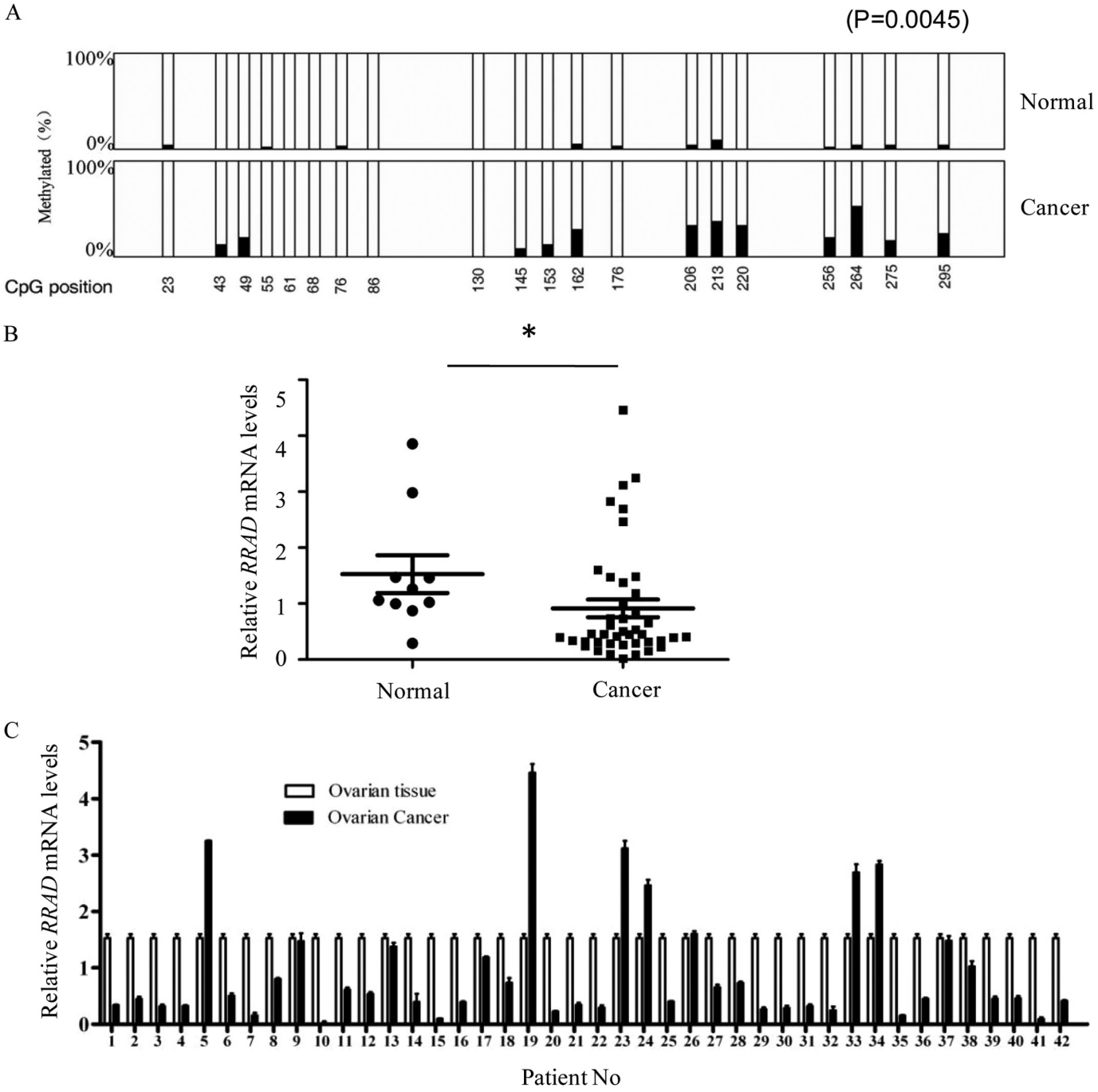


FIGURE 2. ***RRAD* promoter methylation is inversely correlated with expression in epithelial ovarian carcinoma.** *A*, methylation status of the *RRAD* promoter region in normal tissues and epithelial ovarian carcinoma. Each *filled bar* represents the percentage of DNA methylation per CpG site, and the *open bar* represents the percentage of demethylated CpG at each corresponding site (**, $p = 0.0045$). *B*, overall comparison of relative *RRAD* mRNA levels in ovarian cancer ($n = 42$) and normal tissues ($n = 10$). Data are shown as means ± S.E. (*error bars*) (*, $p < 0.05$, Mann-Whitney *U* test). *C*, *RRAD* mRNA levels in individual cancer tissues and the reference tissue sample, which was mixed from 10 normal tissues.

lated genes and 609 down-regulated genes, were identified in T29H with at least 2-fold differences in expression level and false discovery rate value less than 0.0001 (supplemental Table S3). In addition, functional annotation of differentially expressed genes showed that they are enriched in multiple pathways (supplemental Table S4), most of which are involved in cancer and metabolism, including focal adhesion pathway (hsa04510), ribosome pathway (hsa03010), MAPK signaling pathway (hsa04010), PI3K-Akt signaling pathway (hsa04151), VEGF signaling pathway (hsa04370), and pathways in cancer (hsa05200), ECM-receptor interaction (hsa04512), glycosaminoglycan biosynthesis (hsa00532), and *N*-glycan biosynthesis (hsa00510). Our data suggest that Ras transformation affects diversified cancer-related signaling, which may contribute to the carcinogenesis of ovarian cancer.

Subsequently, we investigated the association between DNA methylation and gene expression by integrating the differentially expressed genes and DMRs occurring in the promoter

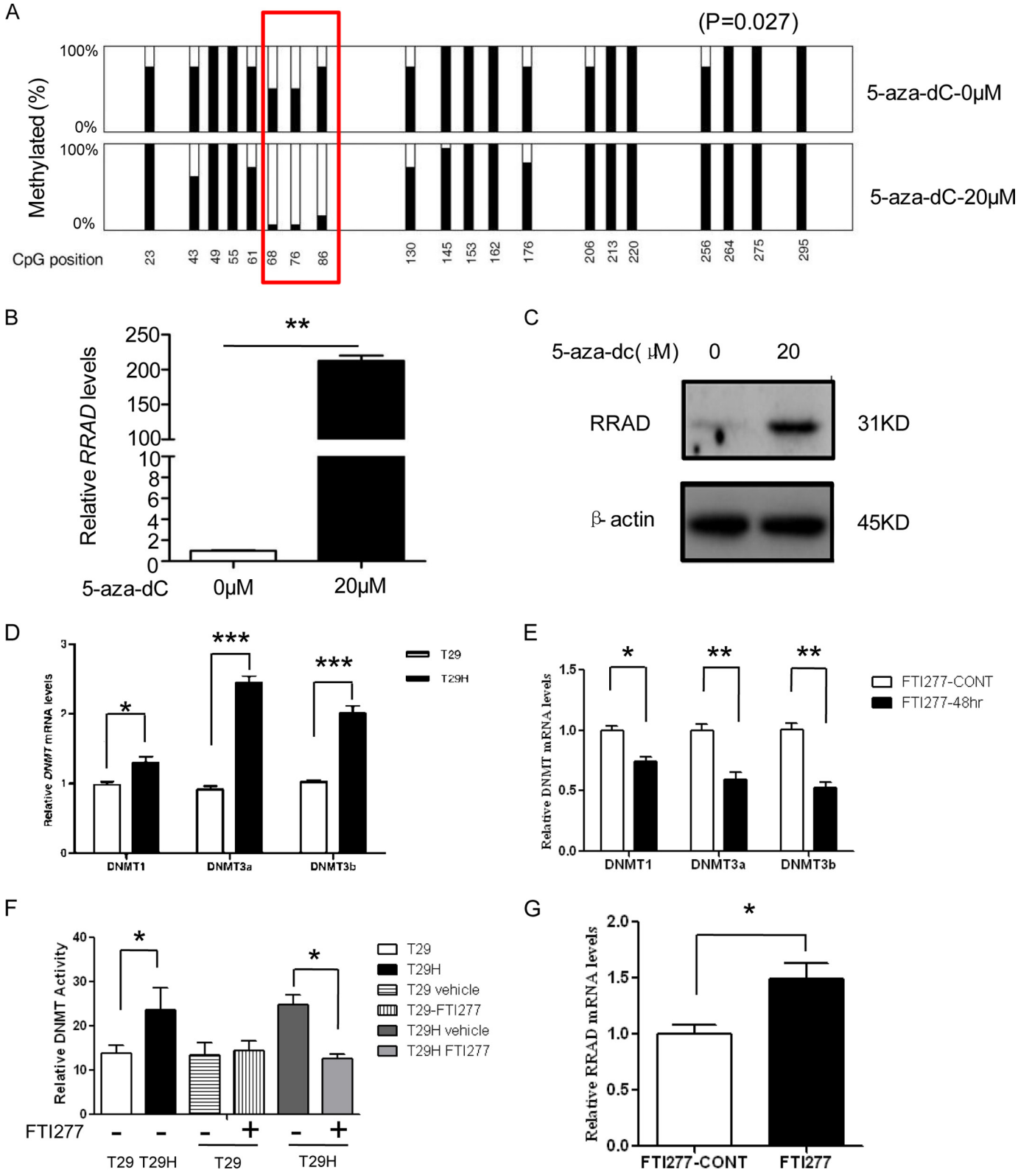


FIGURE 3. **Demethylation of *RRAD* in T29H by 5-aza-dC results in RRAD gene derepression.** *A*, DNA methylation status of the *RRAD* promoter in 5-aza-dC-treated T29H cells. The *red box* marks the "hot spots" that are demethylated upon 5-aza-dC treatment (*, $p = 0.027$). *B*, relative *RRAD* mRNA levels after 5-aza-dC treatment. *C*, RRAD protein levels after treatment with 20 $\mu$M 5-aza-dC. *D*, DNMT mRNA levels in T29H. *E*, relative DNMT mRNA levels after FTI277 treatment. *F*, relative DNMT activity following FTI277 treatment. *G*, relative mRNA levels of *RRAD* following FTI277 treatment. $\beta$-Actin was used as a loading control. Data are shown as means ± S.E. (*error bars*) (*, $p < 0.05$; **, $p < 0.01$; ***, $p < 0.001$).

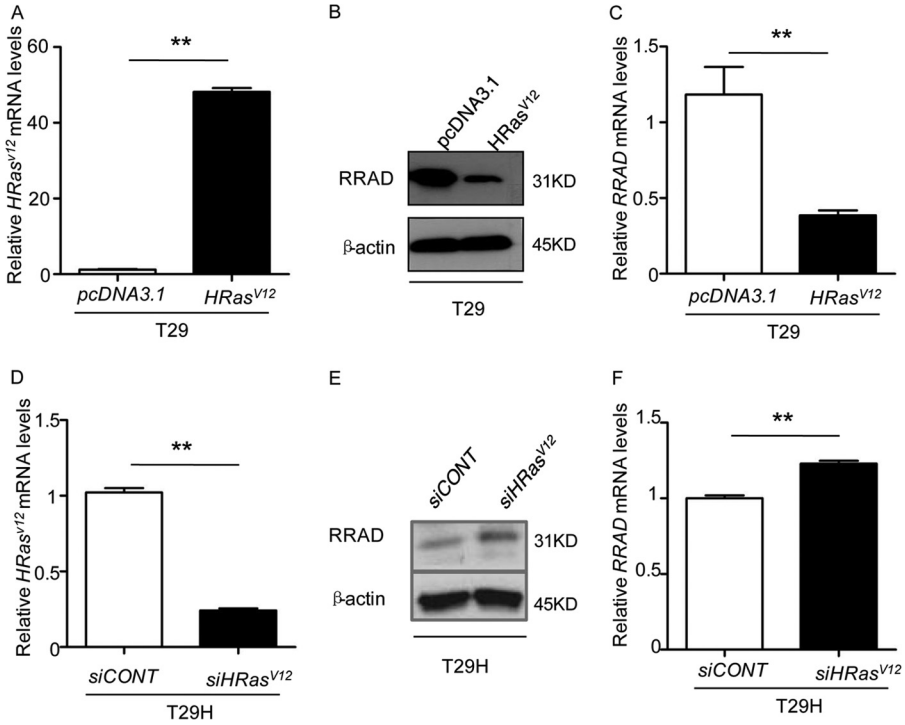


FIGURE 4. **RRAD expression is regulated by HRas$^{V12}$.** *A–C*, overexpression of HRas$^{V12}$ in T29 cells. *A*, *HRas$^{V12}$* transfection efficiency in T29 cells, measured by real-time RT-PCR. *B* and *C*, reduced protein (*B*) and mRNA (*C*) levels of RRAD in HRas$^{V12}$-overexpressing T29 cells. *D–F*, siRNA knockdown of *HRas$^{V12}$* in T29H cells. *D*, transfection efficiency of *HRas$^{V12}$* siRNA in T29H cells. *E* and *F*, up-regulation of RRAD in *HRas$^{V12}$* knockdown T29H cells. *E*, protein level; *F*, relative *RRAD* transcript level. Data are shown as means ± S.E. (*error bars*) (**, $p < 0.01$).

(Fig. 1, *A* and *B*). Interestingly, we observed that the expression level of the *RRAD* gene was inversely correlated with DNA methylation level most significantly. In comparison with T29, the *RRAD* promoter region was ~3.9-fold increased in methylation level and ~7.5-fold decreased in gene expression level in T29H. By employing the bisulfite sequencing and RT-PCR, we confirmed that the RRAD CpG island in the promoter was highly methylated in T29H cells and hypomethylated in T29 cells (Fig. 1*C*). Consistent with these results, RRAD mRNA and its encoded protein levels were dramatically reduced in T29H *versus* T29 by 20-fold (Fig. 1, *D* and *E*).

*Epigenetic Inactivation of RRAD in Human Ovarian Cancer Tissues*—We then characterized the *RRAD* promoter methylation status and the expression level in 42 human ovarian cancers and 10 normal ovarian tissues. As shown in Fig. 2*A*, *RRAD* promoter methylation was significantly increased in ovarian cancer *versus* normal ovarian tissues ($p = 0.0045$). The overall *RRAD* transcript levels were significantly reduced in tumor *versus* normal ovarian tissues (Fig. 2*B*). Because corresponding normal tissue could not be obtained from these 42 cancer patients, *RRAD* transcription was quantified in a mixture of 10 normal ovarian tissues and used as the reference (41). As shown in Fig. 2*C*, the majority (32 of 42) of the cancer tissues tested showed dramatically reduced *RRAD* transcription compared with that in the normal ovarian tissues. These observations suggest that *RRAD* is epigenetically inactivated in ovarian cancer tissues.

*Ras$^{V12}$-mediated Oncogenic Transformation Induces Promoter Hypermethylation and Represses RRAD Expression*—To confirm that RRAD down-regulation in T29H cells was due to promoter hypermethylation, we treated T29H cells with the demethylating agent 5-aza-dC. Indeed, our results revealed that several "hot spots" in the *RRAD* promoter could be remarkably demethylated (at 68, 76, and 86 bp in our bisulfite sequencing region, Fig. 3*A*). Simultaneously, *RRAD* transcription and its protein levels were dramatically increased (Fig. 3, *B* and *C*). These results suggest that promoter hypermethylation represses RRAD expression in T29H cells. Moreover, the expression and activity in DNMTs were significantly increased in T29H cells compared with in T29 cells via RT-PCR and the DNMT activity assay (Fig. 3, *D* and *F*). Consistently, treatment with FTI-277, a specific Ras inhibitor, down-regulated the mRNA levels (Fig. 3*E*) and activities (Fig. 3*F*) of DNMTs, which was concomitant with an up-regulation of RRAD expression (Fig. 3*G*).

T29H cells are derived from T29 cells by introducing an oncogenic HRas$^{V12}$. To exclude the possibility that the difference in promoter methylation and expression of RRAD is due to clonal variation, we transiently transfected T29 cells with *pCMV-Ras$^{V12}$*. As expected, RRAD transcript and protein levels were dramatically reduced upon overexpression of HRas$^{V12}$ in comparison with the empty vector control by more than 3-fold (Fig. 4, *A–C*). A similar effect was observed in other cell lines (data not shown). In addition, *Ras* knockdown in T29H increased RRAD expression (Fig. 4, *D–F*).

*RRAD Down-regulates Glucose Uptake and Lactate Production*—In contrast to normal differentiated cells, which primarily rely on mitochondrial oxidative phosphorylation to generate the energy needed for cellular processes, most cancer cells rely on aerobic glycolysis, a phenomenon termed "the Warburg effect" (13). Aerobic glycolysis, which breaks down glucose to lactate,

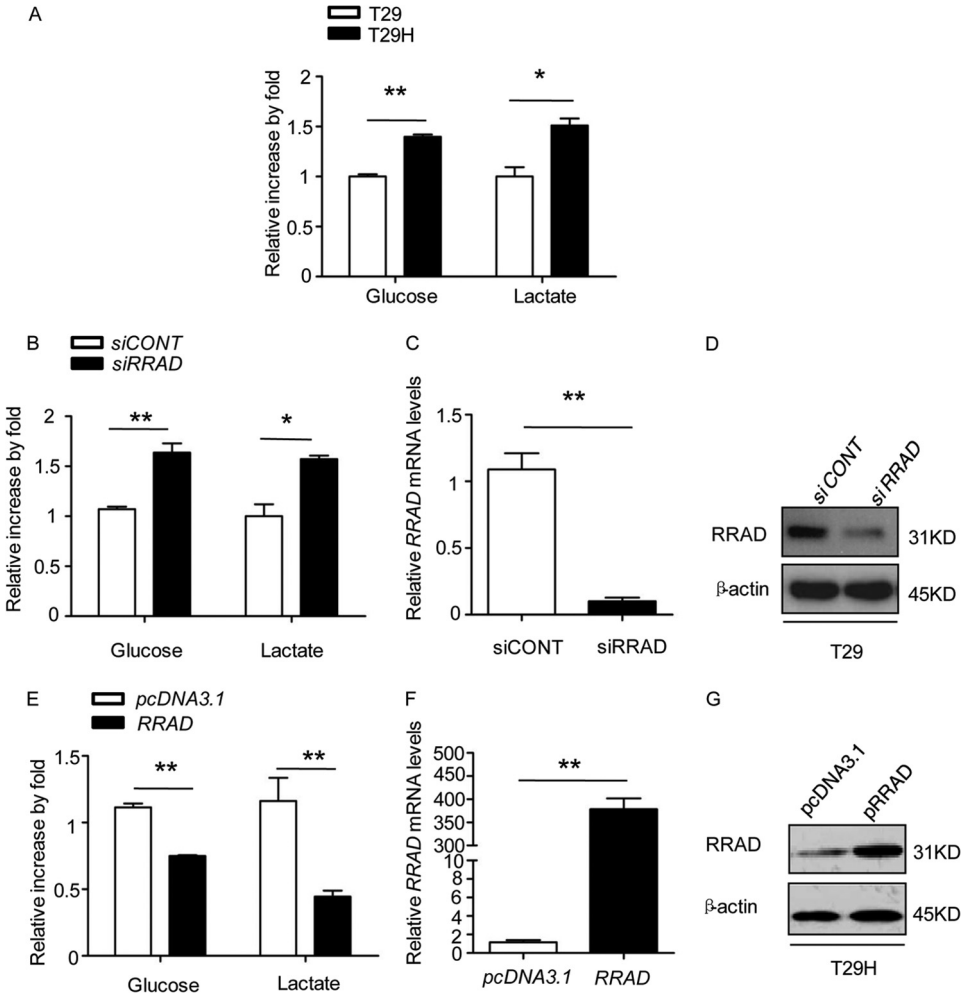


FIGURE 5. **RRAD inhibits glucose uptake and lactate production in ovarian epithelial cells.** *A*, reduced glucose uptake and lactate production in T29 cells *versus* T29H cells that express lower levels of *RRAD*. *B–D*, increased glucose uptake and lactate production in *siRRAD* knockdown T29 cells. *B*, relative glucose and lactate levels. *C*, relative *RRAD* transcript level. *D*, RRAD protein expression level. *E–G*, significantly decreased glucose uptake and lactate production upon *RRAD* overexpression in T29H cells. *E*, relative glucose and lactate levels. *F*, relative *RRAD* transcript level. *G*, RRAD protein expression level. Data are means ± S.E. (*error bars*) (*, $p < 0.05$; **, $p < 0.01$).

is an inefficient way to generate ATP. In general, cancer cells consume more glucose than normal cells to generate sufficient amounts of ATP, and increased glucose uptake and lactate production are hallmarks of cancer cells (13, 14). Therefore, we measured glucose uptake and lactate production in T29 and T29H cells. Our results revealed that $Ras^{V12}$-mediated oncogenic transformation led to an increase in glucose uptake and lactate production (Fig. 5*A*).

Previous studies have shown that overexpression of RRAD in cultured adipocytes and muscle cells results in diminished insulin-stimulated glucose uptake (26), and overexpression of RRAD in muscle tissues of transgenic mice worsens diet-induced insulin resistance and glucose intolerance and reduces plasma triglyceride levels (27). We speculated that increased glucose uptake and lactate production are the consequences of RRAD down-regulation. To test this hypothesis, we knocked down RRAD in T29 cells and found that glucose uptake and lactate production were significantly increased (Fig. 5, *B–D*). Accordingly, overexpression of RRAD in T29H cells, which express relatively low levels of RRAD, led to a significant decrease in glucose uptake and lactate production (Fig. 5, *E–G*), suggesting that RRAD negatively influences aerobic glycolysis.

*RRAD Suppresses the Expression of Glucose Transporters*—Insulin positively regulates glucose uptake by inducing the expression of glucose transporters (42) and may also up-regulate RRAD (43, 44). Therefore, we addressed whether RRAD regulates the expression of glucose transporters. As shown in Fig. 6*A*, the expression levels of most glucose transporters were decreased in *RRAD*-overexpressing T29H cells. Consistent with the observation that RRAD was down-regulated in T29H cells as compared with T29 cells, we found that the expression levels of most glucose transporters were increased in T29H cells as compared with T29 cells (Fig. 6*B*). These results suggest that increased glucose consumption in $Ras^{V12}$-transformed ovarian epithelial cells is probably the consequence of up-regulation of glucose transporters induced by down-regulation of RRAD.

*Overexpression of RRAD in T29H Cells Represses the Oncogenic Potential of $Ras^{V12}$*—Aerobic glycolysis in cancer cells may facilitate the uptake and incorporation of nutrients into the biomass that are necessary for producing a new cell (13). We

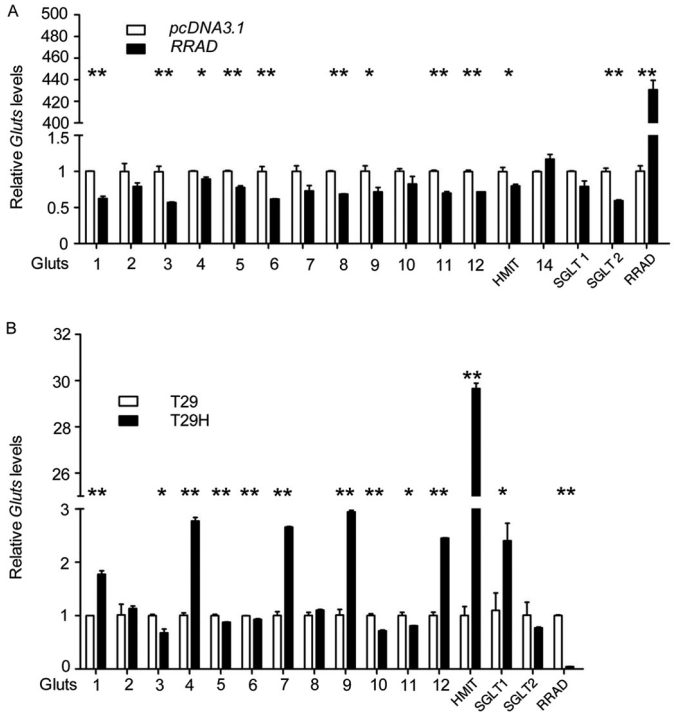


FIGURE 6. **Glucose transporter expression in T29, T29H, and RRAD-overexpressing T29H cells.** *A*, T29H cells were transfected with *pCMV6-XL5 RRAD* or *pcDNA3.1*, and the levels of glucose transporters were determined by real-time RT-PCR 48 h after transfection. *B*, real-time RT-PCR quantification of glucose transporters in T29 and T29H cells. Data are means ± S.E. (*error bars*) (*, $p < 0.05$; **, $p < 0.01$).

demonstrated that $Ras^{V12}$-mediated oncogenic transformation increased glucose uptake and lactate production by down-regulating RRAD expression. Therefore, RRAD derepression may inhibit the oncogenic potential of $Ras^{V12}$. To test this hypothesis, we generated two stable RRAD-overexpressing T29H cell lines, T29H-G7 and T29H-G8 (Fig. 7, *A* and *B*). As shown in Fig. 7*C*, glucose uptake and lactate production were inhibited in RRAD-overexpressing *versus* control T29H cells. We then inoculated T29, T29H, T29H-G7, and T29H-G8 cells into nude mice to examine the effect of RRAD on tumor formation. As reported previously (12), no tumors were observed in mice injected with T29 cells. However, tumor size was significantly smaller in mice inoculated with T29H-G7 and T29H-G8 cells than that in T29H-injected mice (Fig. 7, *D–F*). These results indicated that overexpression of RRAD in T29H cells inhibited the oncogenic potential of $Ras^{V12}$.

## DISCUSSION

Using a well defined human ovarian cancer model, we have demonstrated that RRAD expression was lower in T29H than in T29 cells due to promoter hypermethylation (Fig. 1). Knockdown of $Ras^{V12}$ in T29H cells resulted in up-regulation of the *RRAD* gene (Fig. 4). In addition, we found that DNMTs were up-regulated by $Ras^{V12}$ and that treatment with FTI-277, a specific Ras inhibitor, led to down-regulation of DNMTs in T29H cells (Fig. 3). Taken together, our data suggest that activation of the Ras pathway up-regulates the expression of DNMTs, and Ras-responsive transcription factors may recruit DNMTs to the *RRAD* promoter to induce DNA methylation.

We demonstrated that RRAD inhibited glucose uptake in ovarian epithelial cells (Fig. 5). Consistently, we showed that RRAD repressed lactate production. In addition, we showed that *RRAD* suppressed the expression of glucose transporters. Previous studies have demonstrated that RRAD is associated with calmodulin-dependent protein kinase II, cAMP-dependent protein kinase (PKA), protein kinase C (PKC), and casein kinase II and is phosphorylated by these protein kinases (45, 46). Interestingly, most of these protein kinases are involved in glucose metabolism. Activation of PKA and PKC increased the activity of the $Na^+$-glucose cotransporter SGLT2 (47), and calmodulin-dependent protein kinase II positively regulates glucose uptake by affecting the GLUT4 (glucose transporter 4) expression level (48, 49). Therefore, it is tempting to speculate that RRAD may function downstream for these protein kinases and repress glucose uptake by inhibiting the expression or activities of glucose transporters.

It has been postulated that proliferating and cancer cells could choose glycolysis to efficiently prepare nutrients for fast cell growth (13, 14). Hirabayashi *et al.* (50) reported that a carbohydrate-rich diet promoted Ras/Src-mediated transformation in *Drosophila* and that transformed tumor tissues exhibit diet-mediated insulin sensitivity, increased glucose uptake activity, and resist apoptosis. They also demonstrated that acarbose and AD81 induce tumor cell apoptosis by targeting glucose uptake and Ras/Src AD81, respectively (50). We showed here that $Ras^{V12}$-transformed T29H cells could take up more glucose due to RRAD down-regulation, and overexpression of RRAD in T29H cells inhibited glucose uptake and hence reduced glycolysis (Fig. 5), which displayed a disadvantage for tumor growth. Consistent with this, we found that two stable RRAD-overexpressing T29H cells, T29H-G7 and T29H-G8, took up less glucose and produced less lactate than those T29H did (Fig. 6, *A–C*). In addition, they formed smaller tumors after injection into nude mice (Fig. 6, *D–F*). Considering that RRAD inhibited cell migration in vascular smooth muscle cells (51) and lung cancers (25) and that disruption of RRAD resulted in cell cycle arrest and senescence (20, 52), we propose that *RRAD* is a tumor suppressor gene, which may be a potential new anti-tumor target through regulating RRAD activity.

We also found that RRAD was epigenetically inactivated in ovarian cancer tissues (Fig. 2). The fact that the Ras mutation is found only in a certain subset of ovarian cancers (53) and ~30% of other human cancers (1, 2) suggested that Ras mutation was not the only cause for *RRAD* epigenetic inactivation in cancer. Indeed, Hsiao *et al.* recently demonstrated that RRAD was a direct transcriptional target of p53 and that activation of p53 leads to up-regulation of RRAD (25). Considering the fact that p53 is frequently mutated in cancer cells, we speculate that loss of p53 function is another cause for RRAD down-regulation in tumor tissues. Further efforts should investigate whether mutation of other tumor suppressor genes or oncogenes regulates RRAD expression.

Additionally, we present the first methylome induced by oncogenic Ras through RRBS-seq analysis. 7,567 DMRs were

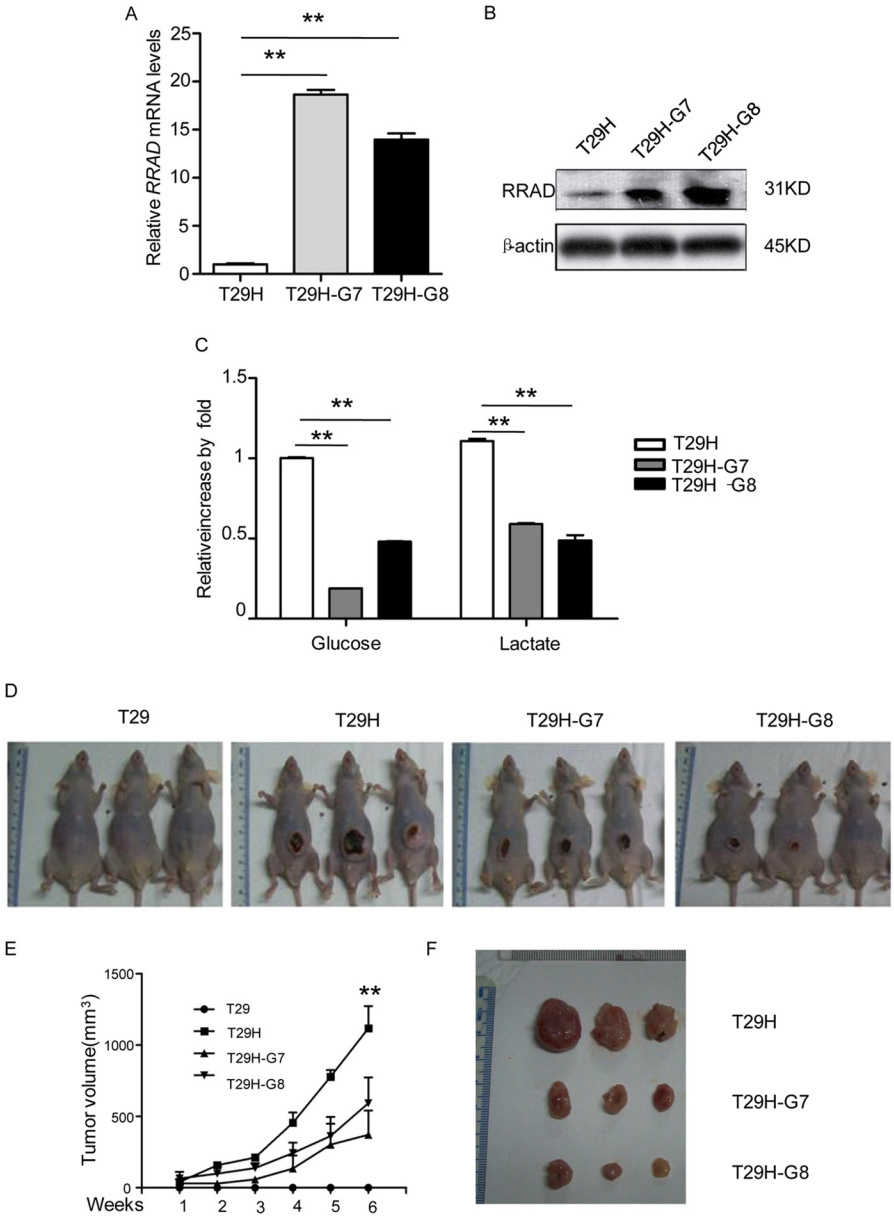


FIGURE 7. **RRAD reduces ovarian tumor growth *in vivo*.** *A*, relative *RRAD* transcript levels in T29H and its stable RRAD-overexpressing derivatives G7 and G8. *B*, RRAD protein expression in T29H and its stable RRAD-overexpressing derivatives. *C*, reduced lactate production in stable RRAD-overexpressing T29H derivatives. *D*, representative images of mice in T29/T29H mouse models 6 weeks after subcutaneous injection. T29 did not form visible tumors; however, mice injected with T29H, T29H-G7, T29H-G8 all formed visible tumors. Due to image quality, images of only 3 mice per treatment are shown. *E*, quantification of tumor volume from subcutaneous injected athymic nude mice, $n = 5$. *F*, representative images of autopsied tumors from T29H, G7, and G8 subcutaneously injected athymic nude mice. Data are means ± S.E. (*error bars*) (**, $p < 0.01$).

identified ($\chi^2$ test, $p < 0.01$, Fold change $\geq 2$) between T29 and T29H through comparison of the methylation levels. We found 1,737 genes, of which promoters were overlapped with DMRs. ClueGO analysis revealed that those genes were enriched in multiple pathways (Table 4), such as the neuroactive ligand-receptor interaction pathway (hsa04080), the calcium signaling pathway (hsa04020), the *o*-glycan biosynthesis pathway (hsa00512), the melanogenesis pathway (hsa04916), the basal cell carcinoma pathway (hsa05217), the fructose and mannose metabolism pathway (hsa00051), the Wnt signaling pathway (hsa04310), the MAPK signaling pathway (hsa04010), the hedgehog signaling pathway (hsa04340), and pathways in cancer (hsa05200; Table 5). Most of them were related to cancer and metabolism. Some of these pathways were reported in ovarian cancers by Huang *et al.* (54). Further, the comparison of the methylation level between T29 and T29H revealed that T29H had slight decrease in the methylation level of C and CpG (Fig. 8*A*), which has been confirmed by the global DNA methylation analysis by the LC-MS/MS method (Fig. 8*B*). The global hypomethylated status in T29H cells was consistent with previous studies in cancers (55), and it further indicated that T29H is a well defined model for human ovarian cancer study.

In summary, we showed that $Ras^{V12}$-mediated oncogenic transformation caused epigenetic inactivation of the *RRAD* gene and that down-regulation of RRAD led to an increase in glucose uptake, which may be associated with the unique

**TABLE 4**
**The distribution of identified DMRs in different genomic features in T29 and T29H**

| Genomic feature | Hypomethylated (T29 > T29H) | Hypermethylated (T29 < T29H) |
|---|---|---|
| Total DMRs | 5,416 | 2,989 |
| 3′-UTR | 84 | 94 |
| 5′-UTR | 581 | 686 |
| CDS | 699 | 649 |
| Intron | 1,002 | 1,147 |
| Promoter | 707 | 1,030 |
| CGI | 1,773 | 1,867 |
| CGI shore | 2,056 | 1,716 |
| Pseudogene | 142 | 32 |
| Intergenic | 1,489 | 1,439 |
| SINE | 1,396 | 506 |
| LINE | 214 | 99 |
| LTR | 325 | 67 |
| Satellite | 97 | 12 |
| Low complexity | 1,044 | 1,054 |
| Simple repeat | 531 | 448 |

**TABLE 5**
**The enriched KEGG term of genes associated with DMRs in the promoter region in T29 and T29H**

| ID | KEGG term | Gene count | Percentage | *p* value |
|---|---|---|---|---|
| | | | % | |
| hsa05032 | Morphine addiction | 25 | 26.88 | 3.57E−08 |
| hsa04080 | Neuroactive ligand-receptor interaction | 45 | 16.36 | 2.10E−06 |
| hsa05033 | Nicotine addiction | 13 | 32.50 | 7.45E−06 |
| hsa05217 | Basal cell carcinoma | 15 | 27.27 | 1.66E−05 |
| hsa04015 | Rap1 signaling pathway | 34 | 15.96 | 6.44E−05 |
| hsa05205 | Proteoglycans in cancer | 35 | 15.56 | 8.66E−05 |
| hsa04010 | MAPK signaling pathway | 38 | 14.79 | 1.31E−04 |
| hsa05412 | ARVC | 16 | 21.62 | 1.87E−04 |
| hsa04727 | GABAergic synapse | 18 | 20.00 | 2.16E−04 |
| hsa04340 | Hedgehog signaling pathway | 12 | 23.53 | 5.23E−04 |
| hsa04724 | Glutamatergic synapse | 20 | 17.24 | 7.65E−04 |
| hsa04916 | Melanogenesis | 18 | 17.82 | 9.30E−04 |
| hsa05034 | Alcoholism | 27 | 15.00 | 9.78E−04 |
| hsa04390 | Hippo signaling pathway | 24 | 15.58 | 0.001073 |
| hsa04723 | Retrograde endocannabinoid signaling | 18 | 17.48 | 0.001178 |
| hsa05030 | Cocaine addiction | 11 | 22.00 | 0.001605 |
| hsa04810 | Regulation of actin cytoskeleton | 30 | 13.95 | 0.00172 |
| hsa04950 | Maturity onset diabetes of the young | 7 | 28.00 | 0.00268 |
| hsa05200 | Pathways in cancer | 40 | 12.23 | 0.003976 |
| hsa04310 | Wnt signaling pathway | 20 | 14.39 | 0.006861 |
| hsa04725 | Cholinergic synapse | 17 | 15.04 | 0.007869 |
| hsa04726 | Serotonergic synapse | 17 | 14.91 | 0.008587 |
| hsa00512 | Mucin type O-Glycan biosynthesis | 7 | 22.58 | 0.009653 |
| hsa04144 | Endocytosis | 26 | 12.81 | 0.01052 |
| hsa05414 | Dilated cardiomyopathy | 14 | 15.56 | 0.011398 |
| hsa04151 | PI3K-Akt signaling pathway | 39 | 11.27 | 0.016555 |
| hsa03320 | PPAR signaling pathway | 11 | 15.94 | 0.01981 |
| hsa04713 | Circadian entrainment | 14 | 14.43 | 0.021138 |
| hsa04020 | Calcium signaling pathway | 22 | 12.15 | 0.030355 |
| hsa05410 | Hypertrophic cardiomyopathy | 12 | 14.46 | 0.031031 |
| hsa04510 | Focal adhesion | 24 | 11.65 | 0.038 |
| hsa04014 | Ras signaling pathway | 26 | 11.45 | 0.038046 |
| hsa05031 | Amphetamine addiction | 10 | 14.71 | 0.042124 |
| hsa04360 | Axon guidance | 16 | 12.60 | 0.044801 |
| hsa05166 | HTLV-I infection | 29 | 11.03 | 0.0455 |

metabolic feature of tumor cells, aerobic glycolysis. Overexpression of RRAD in $Ras^{V12}$-transformed ovarian epithelial cells repressed their oncogenic potential. Therefore, our results suggest that down-regulation of RRAD confers advantages to the proliferation of $Ras^{V12}$-transformed ovarian epithelial cells.

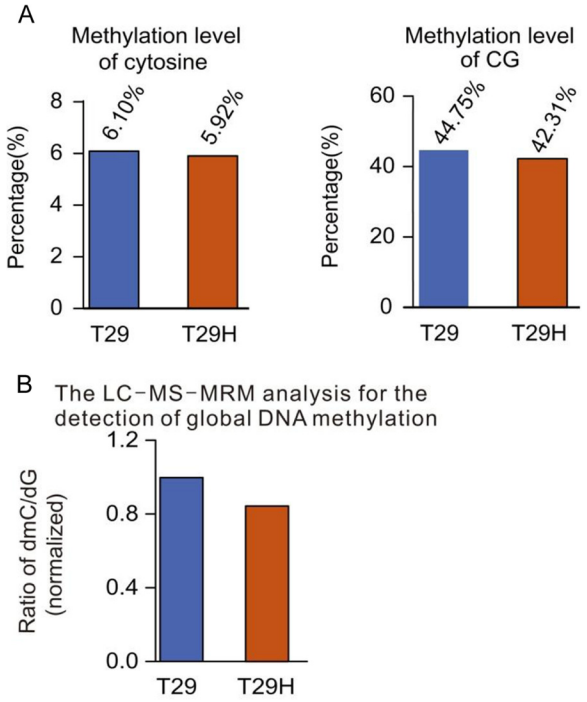


FIGURE 8. **Genomic landscape of DNA methylation in T29 and T29H determined by RRBS-seq.** *A*, the overall methylated level of C and CG in T29 and T29H. *B*, global DNA methylation analysis of methylated level in T29 and T29H using the LC-MS/MS method.

*Acknowledgments—We thank Drs. Jinsong Liu (University of Texas M.D. Anderson Cancer Center) and Jie Du (Beijing Anzhen Hospital, Chinese Capital Medical University) for providing T29 and T29H cell lines. We thank Prof. Zhihai Qin and Dr. Jizhou Lv (Institute of Biophysics, Chinese Academy of Sciences) for expert help in the [$^3$H]glucose uptake assay and Dr. Yi-Ping Li (University of Alabama at Birmingham) and Dr. Scott Edmunds (Beijing Genomics Institute) for critical review of the manuscript.*

## REFERENCES

1. Bos, J. L. (1989) ras oncogenes in human cancer: a review. *Cancer Res.* **49,** 4682–4689
2. Wittinghofer, A. (1998) Signal transduction via Ras. *Biol. Chem.* **379,** 933–937
3. Shiraha, H., Yamamoto, K., and Namba, M. (2013) Human hepatocyte carcinogenesis (review). *Int. J. Oncol.* **42,** 1133–1138
4. Murati, A., Brecqueville, M., Devillier, R., Mozziconacci, M. J., Gelsi-Boyer, V., and Birnbaum, D. (2012) Myeloid malignancies: mutations, models and management. *BMC Cancer* **12,** 304
5. Rusconi, P., Caiola, E., and Broggini, M. (2012) RAS/RAF/MEK inhibitors in oncology. *Curr. Med. Chem.* **19,** 1164–1176
6. Tartaglia, M., and Gelb, B. D. (2010) Disorders of dysregulated signal traffic through the RAS-MAPK pathway: phenotypic spectrum and molecular mechanisms. *Ann. N.Y. Acad. Sci.* **1214,** 99–121
7. Young, T. W., Mei, F. C., Yang, G., Thompson-Lanza, J. A., Liu, J., and Cheng, X. (2004) Activation of antioxidant pathways in ras-mediated oncogenic transformation of human surface ovarian epithelial cells revealed by functional proteomics and mass spectrometry. *Cancer Res.* **64,** 4577–4584
8. Singer, G., Oldt, R., 3rd, Cohen, Y., Wang, B. G., Sidransky, D., Kurman,

R. J., and Shih, I. M. (2003) Mutations in BRAF and KRAS characterize the development of low-grade ovarian serous carcinoma. *J. Natl. Cancer Inst.* **95,** 484–486
9. Varras, M. N., Sourvinos, G., Diakomanolis, E., Koumantakis, E., Flouris, G. A., Lekka-Katsouli, J., Michalas, S., and Spandidos, D. A. (1999) Detection and clinical correlations of ras gene mutations in human ovarian tumors. *Oncology* **56,** 89–96
10. Young, T., Mei, F., Liu, J., Bast, R. C., Jr., Kurosky, A., and Cheng, X. (2005) Proteomics analysis of H-RAS-mediated oncogenic transformation in a genetically defined human ovarian cancer model. *Oncogene* **24,** 6174–6184
11. Mei, F. C., Young, T. W., Liu, J., and Cheng, X. (2006) RAS-mediated epigenetic inactivation of OPCML in oncogenic transformation of human ovarian surface epithelial cells. *FASEB J.* **20,** 497–499
12. Liu, J., Yang, G., Thompson-Lanza, J. A., Glassman, A., Hayes, K., Patterson, A., Marquez, R. T., Auersperg, N., Yu, Y., Hahn, W. C., Mills, G. B., and Bast, R. C., Jr. (2004) A genetically defined model for human ovarian cancer. *Cancer Res.* **64,** 1655–1663
13. Vander Heiden, M. G., Cantley, L. C., and Thompson, C. B. (2009) Understanding the Warburg effect: the metabolic requirements of cell proliferation. *Science* **324,** 1029–1033
14. Hirschhaeuser, F., Sattler, U. G., and Mueller-Klieser, W. (2011) Lactate: a metabolic key player in cancer. *Cancer Res.* **71,** 6921–6925
15. DeBerardinis, R. J., Lum, J. J., Hatzivassiliou, G., and Thompson, C. B. (2008) The biology of cancer: metabolic reprogramming fuels cell growth and proliferation. *Cell Metab.* **7,** 11–20
16. Christofk, H. R., Vander Heiden, M. G., Harris, M. H., Ramanathan, A., Gerszten, R. E., Wei, R., Fleming, M. D., Schreiber, S. L., and Cantley, L. C. (2008) The M2 splice isoform of pyruvate kinase is important for cancer metabolism and tumour growth. *Nature* **452,** 230–233
17. Altenberg, B., and Greulich, K. O. (2004) Genes of glycolysis are ubiquitously overexpressed in 24 cancer classes. *Genomics* **84,** 1014–1020
18. Reynet, C., and Kahn, C. R. (1993) Rad: a member of the Ras family overexpressed in muscle of type II diabetic humans. *Science* **262,** 1441–1444
19. Mo, Y., Midorikawa, K., Zhang, Z., Zhou, X., Ma, N., Huang, G., Hiraku, Y., Oikawa, S., and Murata, M. (2012) Promoter hypermethylation of Ras-related GTPase gene RRAD inactivates a tumor suppressor function in nasopharyngeal carcinoma. *Cancer Lett.* **323,** 147–154
20. Tseng, Y. H., Vicent, D., Zhu, J., Niu, Y., Adeyinka, A., Moyers, J. S., Watson, P. H., and Kahn, C. R. (2001) Regulation of growth and tumorigenicity of breast cancer cells by the low molecular weight GTPase Rad and nm23. *Cancer Res.* **61,** 2071–2079
21. Suzuki, M., Shigematsu, H., Shames, D. S., Sunaga, N., Takahashi, T., Shivapurkar, N., Iizasa, T., Minna, J. D., Fujisawa, T., and Gazdar, A. F. (2007) Methylation and gene silencing of the Ras-related GTPase gene in lung and breast cancers. *Ann. Surg. Oncol.* **14,** 1397–1404
22. Suzuki, M., Toyooka, S., Shivapurkar, N., Shigematsu, H., Miyajima, K., Takahashi, T., Stastny, V., Zern, A. L., Fujisawa, T., Pass, H. I., Carbone, M., and Gazdar, A. F. (2005) Aberrant methylation profile of human malignant mesotheliomas and its relationship to SV40 infection. *Oncogene* **24,** 1302–1308
23. Suzuki, M., Shigematsu, H., Shivapurkar, N., Reddy, J., Miyajima, K., Takahashi, T., Gazdar, A. F., and Frenkel, E. P. (2006) Methylation of apoptosis related genes in the pathogenesis and prognosis of prostate cancer. *Cancer Lett.* **242,** 222–230
24. Sova, P., Feng, Q., Geiss, G., Wood, T., Strauss, R., Rudolf, V., Lieber, A., and Kiviat, N. (2006) Discovery of novel methylation biomarkers in cervical carcinoma by global demethylation and microarray analysis. *Cancer Epidemiol. Biomarkers Prev.* **15,** 114–123
25. Hsiao, B. Y., Chen, C. C., Hsieh, P. C., Chang, T. K., Yeh, Y. C., Wu, Y. C., Hsu, H. S., Wang, F. F., and Chou, T. Y. (2011) Rad is a p53 direct transcriptional target that inhibits cell migration and is frequently silenced in lung carcinoma cells. *J. Mol. Med.* **89,** 481–492
26. Moyers, J. S., Bilan, P. J., Reynet, C., and Kahn, C. R. (1996) Overexpression of Rad inhibits glucose uptake in cultured muscle and fat cells. *J. Biol. Chem.* **271,** 23111–23116
27. Ilany, J., Bilan, P. J., Kapur, S., Caldwell, J. S., Patti, M. E., Marette, A., and Kahn, C. R. (2006) Overexpression of Rad in muscle worsens diet-induced insulin resistance and glucose intolerance and lowers plasma triglyceride level. *Proc. Natl. Acad. Sci. U.S.A.* **103,** 4481–4486
28. Weisenberger, D. J. (2014) Characterizing DNA methylation alterations from The Cancer Genome Atlas. *J. Clin. Invest.* **124,** 17–23
29. Pyla, R., Poulose, N., Jun, J. Y., and Segar, L. (2013) Expression of conventional and novel glucose transporters, GLUT1, -9, -10, and -12, in vascular smooth muscle cells. *Am. J. Physiol. Cell Physiol.* **304,** C574–C589
30. Gao, F., Liu, X., Wu, X. P., Wang, X. L., Gong, D., Lu, H., Xia, Y., Song, Y., Wang, J., Du, J., Liu, S., Han, X., Tang, Y., Yang, H., Jin, Q., Zhang, X., and Liu, M. (2012) Differential DNA methylation in discrete developmental stages of the parasitic nematode *Trichinella spiralis*. *Genome Biol.* **13,** R100
31. Yang, J., Corsello, T. R., and Ma, Y. (2012) Stem cell gene SALL4 suppresses transcription through recruitment of DNA methyltransferases. *J. Biol. Chem.* **287,** 1996–2005
32. Marbach, E. P., and Weil, M. H. (1967) Rapid enzymatic measurement of blood lactate and pyruvate: use and significance of metaphosphoric acid as a common precipitant. *Clin. Chem.* **13,** 314–325
33. Gu, H., Bock, C., Mikkelsen, T. S., Jäger, N., Smith, Z. D., Tomazou, E., Gnirke, A., Lander, E. S., and Meissner, A. (2010) Genome-scale DNA methylation mapping of clinical samples at single-nucleotide resolution. *Nat. Methods* **7,** 133–136
34. Li, R., Li, Y., Kristiansen, K., and Wang, J. (2008) SOAP: short oligonucleotide alignment program. *Bioinformatics* **24,** 713–714
35. Li, Y., Zhu, J., Tian, G., Li, N., Li, Q., Ye, M., Zheng, H., Yu, J., Wu, H., Sun, J., Zhang, H., Chen, Q., Luo, R., Chen, M., He, Y., Jin, X., Zhang, Q., Yu, C., Zhou, G., Sun, J., Huang, Y., Zheng, H., Cao, H., Zhou, X., Guo, S., Hu, X., Li, X., Kristiansen, K., Bolund, L., Xu, J., Wang, W., Yang, H., Wang, J., Li, R., Beck, S., Wang, J., and Zhang, X. (2010) The DNA methylome of human peripheral blood mononuclear cells. *PLoS Biol.* **8,** e1000533
36. Wang, T., Liu, Q., Li, X., Wang, X., Li, J., Zhu, X., Sun, Z. S., and Wu, J. (2013) RRBS-Analyser: a comprehensive web server for reduced representation bisulfite sequencing data analysis. *Hum. Mutat.* **34,** 1606–1610
37. Langmead, B., Trapnell, C., Pop, M., and Salzberg, S. L. (2009) Ultrafast and memory-efficient alignment of short DNA sequences to the human genome. *Genome Biol.* **10,** R25
38. Morrissy, A. S., Morin, R. D., Delaney, A., Zeng, T., McDonald, H., Jones, S., Zhao, Y., Hirst, M., and Marra, M. A. (2009) Next-generation tag sequencing for cancer gene expression profiling. *Genome Res.* **19,** 1825–1835
39. Audic, S., and Claverie, J. M. (1997) The significance of digital gene expression profiles. *Genome Res.* **7,** 986–995
40. Noushmehr, H., Weisenberger, D. J., Diefes, K., Phillips, H. S., Pujara, K., Berman, B. P., Pan, F., Pelloski, C. E., Sulman, E. P., Bhat, K. P., Verhaak, R. G., Hoadley, K. A., Hayes, D. N., Perou, C. M., Schmidt, H. K., Ding, L., Wilson, R. K., Van Den Berg, D., Shen, H., Bengtsson, H., Neuvial, P., Cope, L. M., Buckley, J., Herman, J. G., Baylin, S. B., Laird, P. W., Aldape, K., and Cancer Genome Atlas Research Network (2010) Identification of a CpG island methylator phenotype that defines a distinct subgroup of glioma. *Cancer Cell* **17,** 510–522
41. Wei, S. H., Chen, C. M., Strathdee, G., Harnsomburana, J., Shyu, C. R., Rahmatpanah, F., Shi, H., Ng, S. W., Yan, P. S., Nephew, K. P., Brown, R., and Huang, T. H. (2002) Methylation microarray analysis of late-stage ovarian carcinomas distinguishes progression-free survival in patients and identifies candidate epigenetic markers. *Clin. Cancer Res.* **8,** 2246–2252
42. Cormont, M., and Le Marchand-Brustel, Y. (2001) The role of small G-proteins in the regulation of glucose transport (review). *Mol. Membr. Biol.* **18,** 213–220
43. Laville, M., Auboeuf, D., Khalfallah, Y., Vega, N., Riou, J. P., and Vidal, H. (1996) Acute regulation by insulin of phosphatidylinositol-3-kinase, Rad, Glut 4, and lipoprotein lipase mRNA levels in human muscle. *J. Clin. Invest.* **98,** 43–49
44. Ducluzeau, P. H., Perretti, N., Laville, M., Andreelli, F., Vega, N., Riou, J. P., and Vidal, H. (2001) Regulation by insulin of gene expression in human skeletal muscle and adipose tissue. Evidence for specific defects in type 2 diabetes. *Diabetes* **50,** 1134–1142
45. Moyers, J. S., Zhu, J., and Kahn, C. R. (1998) Effects of phosphorylation on function of the Rad GTPase. *Biochem. J.* **333,** 609–614

46. Zhu, J., Reynet, C., Caldwell, J. S., and Kahn, C. R. (1995) Characterization of Rad, a new member of Ras/GTPase superfamily, and its regulation by a unique GTPase-activating protein (GAP)-like activity. *J. Biol. Chem.* **270,** 4805–4812
47. Ghezzi, C., and Wright, E. M. (2012) Regulation of the human $Na^+$-dependent glucose cotransporter hSGLT2. *Am. J. Physiol. Cell Physiol.* **303,** C348–C354
48. Ojuka, E. O., Goyaram, V., and Smith, J. A. (2012) The role of CaMKII in regulating GLUT4 expression in skeletal muscle. *Am. J. Physiol.* **303,** E322–E331
49. Ozcan, L., Wong, C. C., Li, G., Xu, T., Pajvani, U., Park, S. K., Wronska, A., Chen, B. X., Marks, A. R., Fukamizu, A., Backs, J., Singer, H. A., Yates, J. R., 3rd, Accili, D., and Tabas, I. (2012) Calcium signaling through CaMKII regulates hepatic glucose production in fasting and obesity. *Cell Metab.* **15,** 739–751
50. Hirabayashi, S., Baranski, T. J., and Cagan, R. L. (2013) Transformed *Drosophila* cells evade diet-mediated insulin resistance through wingless signaling. *Cell* **154,** 664–675
51. Fu, M., Zhang, J., Tseng, Y. H., Cui, T., Zhu, X., Xiao, Y., Mou, Y., De Leon, H., Chang, M. M., Hamamori, Y., Kahn, C. R., and Chen, Y. E. (2005) Rad GTPase attenuates vascular lesion formation by inhibition of vascular smooth muscle cell migration. *Circulation* **111,** 1071–1077
52. Lee, I., Yeom, S. Y., Lee, S. J., Kang, W. K., and Park, C. (2010) A novel senescence-evasion mechanism involving Grap2 and cyclin D interacting protein inactivation by Ras associated with diabetes in cancer cells under doxorubicin treatment. *Cancer Res.* **70,** 4357–4365
53. Kalamanathan, S., Bates, V., Lord, R., and Green, J. A. (2011) The mutational profile of sporadic epithelial ovarian carcinoma. *Anticancer Res.* **31,** 2661–2668
54. Huang, R. L., Gu, F., Kirma, N. B., Ruan, J., Chen, C. L., Wang, H. C., Liao, Y. P., Chang, C. C., Yu, M. H., Pilrose, J. M., Thompson, I. M., Huang, H. C., Huang, T. H., Lai, H. C., and Nephew, K. P. (2013) Comprehensive methylome analysis of ovarian tumors reveals hedgehog signaling pathway regulators as prognostic DNA methylation biomarkers. *Epigenetics* **8,** 624–634
55. Zeimet, A. G., Fiegl, H., Goebel, G., Kopp, F., Allasia, C., Reimer, D., Steppan, I., Mueller-Holzner, E., Ehrlich, M., and Marth, C. (2011) DNA ploidy, nuclear size, proliferation index and DNA-hypomethylation in ovarian cancer. *Gynecol. Oncol.* **121,** 24–31